

# **Evaluation of bioprosthetic heart valve failure using a matrix-fibril shear stress transfer approach**

**Afshin Anssari-Benam<sup>\*</sup>, Asa H. Barber and Andrea Bucchi**

School of Engineering,  
University of Portsmouth,  
Anglesea Road,  
Portsmouth PO1 3DJ  
United Kingdom

\* Address for correspondence:

Afshin Anssari-Benam,  
School of Engineering,  
University of Portsmouth,  
Anglesea Road,  
Portsmouth PO1 3DJ  
United Kingdom

Tel: ++44 (0)23 9284 2187

Fax: ++44 (0)23 9284 2351

E-mail: [afshin.anssari-benam@port.ac.uk](mailto:afshin.anssari-benam@port.ac.uk)

Word count: 4021

## Abstract

A matrix-fibril shear stress transfer approach is devised and developed in this paper to analyse the primary biomechanical factors which initiate the structural degeneration of the bioprosthetic heart valves (BHVs). Using this approach, the critical length of the collagen fibrils  $l_c$  and the interface shear acting on the fibrils in both BHV and natural aortic valve (AV) tissues under physiological loading conditions are calculated and presented. It is shown that the required critical fibril length to provide effective reinforcement to the natural AV and the BHV tissue is  $l_c = 25.36 \mu\text{m}$  and  $l_c = 66.81 \mu\text{m}$ , respectively. Furthermore, the magnitude of the required shear force acting on fibril interface to break a cross-linked fibril in the BHV tissue is shown to be  $38 \mu\text{N}$ , while the required interfacial force to break the bonds between the fibril and the surrounding extracellular matrix is  $31 \mu\text{N}$ . Direct correlations are underpinned between these values and the ultimate failure strength and the failure mode of the BHV tissue compared with the natural AV, and are verified against the existing experimental data. The analyses presented in this paper explain the role of fibril interface shear and critical length in regulating the biomechanics of the structural failure of the BHVs, for the first time. This insight facilitates further understanding into the underlying causes of the structural degeneration of the BHVs *in vivo*.

**Key words:** bioprosthetic heart valve, aortic valve, fibre-reinforced composite materials, structural failure, critical length, fibril interface shear.

# Evaluation of bioprosthetic heart valve failure using a matrix-fibril shear stress transfer approach

## Background

Bioprosthetic heart valves (BHVs) continue to be the dominant clinical solution in adult heart valve replacements. Their structural fabric is composed of biologically derived heterograft biomaterials, undergone chemical (glutaraldehyde) treatment to render minimal immunological reactions from the host body after implantation. Despite this favourable immunological attribute, biomechanical properties of BHVs have been shown to be significantly distinct to those of the native valve. Studies have characterised higher stiffness for BHV specimens compared with native aortic valve (AV) tissue samples under both uniaxial and biaxial tension (for example see references [1-3]), while reporting lower failure stresses/strains [4-6].

Limited functional durability of the BHVs *in vivo* has also been well documented [7-9], with most of the BHVs showing failure often within the first 5-10 years after implantation. Combination of biotic and mechanical factors are thought to contribute to the underlying causes of this durability limitation [8, 10]. However, the latter is cited as the prominent cause, as approximately 90% of all BHVs fabricated from porcine AVs exhibit structural failure as a direct result of mechanical factors such as fatigue and mechanical damage [7, 11]. The main mode of failure has been shown to be the delamination between collagen fibre layers, i.e. disruption of the fibre architecture of the BHV tissue while the fibres themselves remain intact and retain their alignment as a whole [10, 12].

These distinctions between the biomechanical properties of the BHV and the native AV are widely attributed to the increased density of crosslinks between collagen fibrils in BHV tissue, incurring as a result of glutaraldehyde fixation. However, quantitative analyses and descriptions to elucidate how these alterations in the microstructure may translate to the above-cited differences between the tissue-level properties of the two valve types are less well elaborated in the literature. In particular, analytical interpretations to explain the disparity in the failure characteristics of the BHV versus the native AV, both in terms of the reported values and the failure mode, based on the differences in their microstructural attributes resulting from fixation have been largely unaddressed. Such knowledge would

provide a better understanding of the underlying biomechanics of the BHV structural degeneration *in vivo*, and would be a key contributor to the development of improved BHV tissue biomaterials to facilitate prolonged durability [7].

A novel interpretation of the differences between the reported failure characteristics of the BHV and the native AV tissues in the literature is presented in this paper, by employing the theory of fibre-reinforced composite materials. In light of the concept of fibre critical length  $l_c$ , the primary cause of these differences are shown to be linked to the altered shear at the collagen fibrils' interface as a result of glutaraldehyde fixation and creation of new crosslinks between fibrils in BHV tissue compared with the native AV. Calculations are made to show how the ultimate failure stress of the fixed tissue is predicted from that of the natural tissue by taking the respective critical lengths into account. Based on these analyses, the underlying cause in initiating the fatigue-induced structural degeneration of BHV tissue in the form of delamination between collagen fibril layers is explained. To avoid the inherent and unwanted effects of fixation on the biomechanics of the failure of the BHVs discussed here, an alternative approach to the existing chemical-treatment based methods for BHV fabrication is suggested.

### **Aortic valve as a fibre-reinforced composite material**

The native AV is comprised of three coapting soft collagenous connective cardiac tissues, referred to as leaflets, and is located between the left ventricle and the aorta. The AV essentially acts as a check valve to prevent the retrograde flow of blood from the aorta to the heart at each cardiac cycle. The anatomy of the valve along with an intact AV leaflet and a schematic of its structure is shown in Figure 1. Each leaflet consists of three morphological distinct layers, namely fibrosa, spongiosa and ventricularis. The predominance of the extracellular matrix (ECM) elements of the AV is layer specific. Fibrosa mainly accommodates the collagen constituent of the valve, elastin is mainly localised in the ventricularis, and spongiosa is mainly comprised of glycosaminoglycans (GAGs).

Given the significantly lower thickness (typically ranging from 0.5 mm to 0.7 mm [3, 16, 17]) of the AV leaflet compared to its other two dimensions, and in particular the very low thickness of the fibrosa layer (0.2 mm [16]), it has been admissible from a biomechanics point of view to consider AV leaflet as a planar tissue [13, 17, 18]. Collagen fibres are also

considered to have an in-plane distribution, primarily aligned in the circumferential direction (Figure 1d) of the leaflet [13, 18, 19], and embedded within GAGs (Figure 1e) which act as a gel-like viscous ground substance [17, 20, 21].

This structure models a strong resemblance to fibre-reinforced composite materials. The application of the theory of fibre-reinforced composite materials to collagenous soft tissues has been devised and demonstrated through the works of Aspden (1994a), Aspden (1994b), and Goh et al. (2003) [20-22], amongst others. Same representation is adopted in the current study for the purpose of the analysis carried out and presented in this paper, with the caveat that the reinforcing elements in AV tissue are collagen *fibrils*. The collagen fibrils are considered analogous to reinforcing fibres in engineering composite theory, despite the variation in length scales where engineering fibres are typically two orders of magnitude larger than diameters (~100 nm) of collagen fibrils.

### Stress on a fibril and its critical length based on fibre composite materials theory

Considering that fibrils assume a cylindrical shape when straight, the equations of elasticity describing displacement and stress fields in a fibril under equilibrium in the most general case are given by:

$$\begin{aligned}
 (\lambda + 2\mu) \frac{\partial^2 u}{\partial r^2} + (\lambda + 2\mu) \frac{\partial}{\partial r} \left( \frac{u}{r} \right) + \mu \frac{\partial^2 u}{\partial z^2} + (\lambda + \mu) \frac{\partial^2 w}{\partial r \partial z} &= 0 & \text{(a)} \\
 \frac{\partial}{\partial r} \left( \frac{1}{r} \frac{\partial(rv)}{\partial r} \right) + \frac{\partial^2 v}{\partial z^2} &= 0 & \text{(b)} \\
 (\lambda + \mu) \left( \frac{\partial^2 u}{\partial r \partial z} + \frac{1}{r} \frac{\partial u}{\partial z} \right) + \mu \left( \frac{\partial^2 w}{\partial r^2} + \frac{1}{r} \frac{\partial w}{\partial r} \right) + (\lambda + 2\mu) \frac{\partial^2 w}{\partial z^2} &= 0 & \text{(c)} \\
 \sigma_{rr} = (\lambda + 2\mu) \frac{\partial u}{\partial r} + \lambda \frac{u}{r} + \lambda \frac{\partial w}{\partial z}, \quad \tau_{rz} = \mu \left( \frac{\partial w}{\partial r} + \frac{\partial u}{\partial z} \right) & & \text{(d)} \\
 \sigma_{zz} = \lambda \frac{\partial u}{\partial r} + \lambda \frac{u}{r} + (\lambda + 2\mu) \frac{\partial w}{\partial z}, \quad \tau_{\varphi z} = \mu \frac{\partial v}{\partial z} & & \text{(e)} \\
 \sigma_{\varphi\varphi} = (\lambda + 2\mu) \frac{u}{r} + \lambda \frac{\partial u}{\partial r} + \lambda \frac{\partial w}{\partial z}, \quad \tau_{r\varphi} = \mu \left( \frac{\partial u}{\partial r} - \frac{v}{r} \right) & & \text{(f)}
 \end{aligned} \tag{1}$$

where  $r$ ,  $\varphi$  and  $z$  are the cylindrical coordinates,  $u$ ,  $v$  and  $w$  denote the radial, circumferential and longitudinal displacements,  $\sigma$  and  $\tau$  are the normal and shear stresses respectively, and

$\lambda$  and  $\mu$  are Lamé's constants. Note that  $\frac{\partial u}{\partial \varphi} = \frac{\partial v}{\partial \varphi} = \frac{\partial w}{\partial \varphi} = 0$  due to the axis-symmetry of cylinder.

The assumption of linear elasticity for collagen fibril is qualified by noting the relevant experimental stress-strain data in the literature and microstructural-based models which incorporate the behaviour of single fibrils. Studies investigating the mechanical properties of single collagen fibrils suggest that, while the fibril undergoes relatively large deformations before failure, linear regressions accurately characterise the relationship between the stress and strain of the fibrils, particularly at large strains [23-28]. Additionally, microstructural models of tissue behaviour based on gradual fibril recruitment have shown accurate characterisation of the tissue-level behaviour by considering fibrils as linear elastic units [19].

Differentiating equation (1a) with respect to  $z$  and equation (1c) with respect to  $r$ , using the notation  $L^2$  for  $\frac{\partial}{\partial r} \frac{1}{r} \frac{\partial}{\partial r} r$  and  $D^2$  for  $\frac{\partial^2}{\partial z^2}$ , equations (1a) to (1c) can be re-written as:

$$\begin{aligned} ((\lambda + 2\mu)L^2 + \mu D^2) \frac{\partial u}{\partial z} + (\lambda + \mu) D^2 \frac{\partial w}{\partial r} &= 0 & \text{(a)} \\ (L^2 + D^2)v &= 0 & \text{(b)} \\ (\lambda + \mu)L^2 \frac{\partial u}{\partial z} + (\mu L^2 + (\lambda + 2\mu)D^2) \frac{\partial w}{\partial r} &= 0 & \text{(c)} \end{aligned} \quad (2)$$

Eliminating  $\frac{\partial u}{\partial z}$  between (2a) and (2c), one finds that all above three equations satisfy the general partial differential equation of the form:

$$(L^2 + D^2)^2 V = 0 \quad (3)$$

This differential equation is equivalent to Laplace's equation in cylindrical coordinate, partially differentiated with respect to  $r$ :

$$\frac{\partial}{\partial r} \left( \frac{1}{r} \frac{\partial}{\partial r} r \frac{\partial V}{\partial r} + \frac{1}{r^2} \frac{\partial^2 V}{\partial \varphi^2} + \frac{\partial^2 V}{\partial z^2} \right) = 0 \Rightarrow (L^2 + D^2) \frac{\partial V}{\partial r} = 0 \quad (4)$$

and therefore the same solution applies. Under the assumptions that:

- (i) the fibril is not subjected to torsion;
- (ii) the surrounding matrix can only generate shear stress on the lateral surface of the fibril;

- (iii) the ensuing shear stress remains uniform along the fibril length;
- (iv) the displacement field (as a result of the applied shear) is an odd function of fibril length;
- (v) the fibril is isotropic (despite the fact that the helical structure of collagen is likely to give rise to strong anisotropy); and
- (vi) the ratio of fibril diameter to fibril length is very small;

the above equation is solved to obtain the relationship between the longitudinal stress  $\sigma_{zz}$  of a fibril and the applied shear stress on its lateral surface  $\tau_{rz}$  as [21, 29]:

$$\sigma_{zz} = \frac{\tau_{rz} l}{r} \quad (5)$$

where  $r$  and  $l$  are the radius and length of a fibril, respectively. Maximum reinforcement is obtained when a fibril is capable of withstanding longitudinal stresses up to its ultimate failure stress,  $(\sigma_{zz})_{failure}$ . This is achieved if the fibril is longer than a minimum length, also known as the critical length  $l_c$ , which is calculated as:

$$l_c = \frac{r (\sigma_{zz})_{failure}}{\tau_{rz}} \quad (6)$$

We note that collagen fibrils are considered to endure only tensile tension, along their longitudinal axis. Therefore, while the fibrils may possess different mechanical properties in the transverse direction, this anisotropy is not considered to play a determining role in the contribution of the fibrils to the mechanical properties of the subject soft tissues. The assumption of elastic isotropy of collagen fibrils have been previously utilised and corroborated for various planar tissues, including the AV [19]. Equations (5) and (6) therefore provide admissible accuracy for preliminary analysis and application to collagenous soft tissues, as demonstrated in references [20] and [21].

### **Shear stress on a fibril in AV**

Shear stresses are generated at the interface between a residing fibril and the surrounding matrix (i.e. the lateral surface area of the fibril) when collagenous soft tissues are subjected to deformation, as a result of dissipative kinetics of fibril-fibril sliding [30] and viscous-like effect of the ground substance GAG [17, 20, 31]. In a recent study, we developed a rheological model to estimate those dissipative effects in AV tissue, using a Kelvin-Voigt

based model by quantifying the equivalent viscous coefficient ( $\eta$ ) under various elongation rates ( $\dot{\lambda}$ ) [17]. The calculated  $\eta$  values in circumferential loading direction, as the prominent load-bearing direction of the valve tissue, are presented in Figure 2a. To estimate the corresponding value of  $\eta$  under physiological loading condition where  $\dot{\lambda} \approx 2.5 \text{ s}^{-1}$  [32], a bi-exponential function of the form  $\eta(\dot{\lambda}) = a \exp b\dot{\lambda} + c \exp d\dot{\lambda}$  was used to model the variation of  $\eta$  versus  $\dot{\lambda}$ , described in Appendix A, where  $a$ ,  $b$ ,  $c$  and  $d$  are coefficients calculated by fitting the function to the  $(\dot{\lambda}, \eta)$  data. Using MATLAB<sup>®</sup> to perform the fitting procedure (see Appendix A), the value of  $\eta$  at  $\dot{\lambda} = 2.5 \text{ s}^{-1}$  was approximated to be 0.0145 MPa s (Figure 2a). The ensuing shear stress is calculated by  $\tau = 2\eta V$ , where  $V$  is the rate of deformation tensor, and in the case of uniaxial loading is given by  $V = \frac{\dot{\lambda}}{\lambda}$  [17]. Noting that the *in vivo* value of  $\lambda$  for the functioning valve in the circumferential direction under physiological conditions is approximately 1.101 [33], the shear stress is calculated to be  $\tau = 0.066 \text{ MPa}$ .

The fibril critical length in the natural AV is calculated using equation (6) and requires numerical values for the fibril radius  $r$  as well as the fibril failure stress. Fibril geometry was obtained from conventional light microscopy histological images of micro-sectioned samples of unloaded natural porcine AV specimens (prepared within 2 hours of slaughter from a local abattoir), stained with Picro Sirius Red for collagen. A customised code developed in MATLAB<sup>®</sup> was used to convert images into grey scale with enhanced contrast to facilitate the segmentation of the wavy fibrils from the background. Regions of interest were then specified in each processed image and individual fibril geometries were identified. Numerical data regarding the properties of interest of each fibril including its radius and crimped length, as well as the  $x$  and  $y$  coordinates of its wavy profile, were subsequently extracted. Using the data obtained from the overall regions of interest in processed images, histogram of the values of the radius and crimped length for the entire processed fibril population were produced. The average fibril radius and crimped length were calculated to be  $r = 275 \text{ nm}$  and  $l_0 = 56.39 \text{ }\mu\text{m}$ , respectively. A typical histological and post-processed image is shown in Figure 3, including the reconstructed histograms of the radius and crimped length of the fibril population, along with the  $x$  and  $y$  coordinates of the profile of a representative fibril.

The failure stress of collagen fibrils were found assuming that the stress-strain relationship of a fibril could be approximated by  $\sigma = E\varepsilon$ , such that estimation of  $\sigma_{failure}$  can

be made by knowing the values of  $E$  and  $\varepsilon_{failure}$ . The elastic modulus of collagen fibrils in AV has been reported to be  $E = 101.22$  MPa [13]. We note that this elastic modulus value for AV fibrils is relatively low compared to fibrils obtained from other collagenous tissue sources such as from bone [27], but is consistent with values from other valve tissues [34]. The failure strain of a fibril has been reported to range from 4% up to 9% [24, 26, 35]. Assuming an average value of  $\varepsilon_{failure} = 6\%$  [27], the  $\sigma_{failure}$  may be estimated as  $\sigma_{failure} = 6.07$  MPa. Substituting these values into equation (6) gives a fibril critical length in AV tissue of  $l_c = 25.36$   $\mu\text{m}$ .

### **The effects of Glutaraldehyde treatment (fixation)**

BHV tissues undergo glutaraldehyde treatment (fixation) to minimise the provocation of immunologic reactions of the host body. However, this process also tightly crosslinks the extracellular matrix (ECM) proteins, through new covalent bonds that are created between the primary amine groups of proteins and the reactive aldehyde chains of the glutaraldehyde [12]. To quantify the effects of these microstructural changes on the shear stress acting on the interface of a fibril and on its critical length, we fitted our rheological model in [17] to the experimental data presented in various studies where the stress-strain curves were reported for both normal and fixed tissues, including that by Thubrikar et al. (1980), Lee et al. (1984), and Purinya et al. (1994) [2, 4, 5]. A typical fit is shown in Figure 2b. The modelling outcomes indicated that the resulting values for  $\eta$  in fixed tissue were consistently up to 5 times higher than that of a normal tissue. Since the fixation process does not affect the geometrical properties of the fibrils, the shear stress acting on fibril's interface in BHV tissue is correspondingly up to 5 times higher than its equivalent in normal tissue. Therefore the value for fibril shear stress in BHV is assumed to be higher than the AV case at  $\tau = 0.32$  MPa.

The major collagen component in AV ECM is collagen type I, constituting approximately 74% of the overall collagen content of the valve [36]. The mechanical properties of cross-linked type I collagen fibril are reported to be  $E = 250$  MPa to 500 MPa, while the failure strain ranges from  $\varepsilon_{failure} = 13\%$  to  $\varepsilon_{failure} = 19\%$  [23, 37]. Taking the average value for failure strain as  $\varepsilon_{failure} = 16\%$ , the failure stress of a cross-linked fibril may go up to

$\sigma_{failure} = 80$  MPa. Therefore, the fibril critical length in the fixed BHV tissue is calculated using equation (6) as  $l_c = 66.81$   $\mu\text{m}$ .

### A point of caution

Characterisation of fibril length and radius, and hence the estimation of the critical length of cross-linked and natural AV fibrils presented here are based, in part, on the histological images of micro-sectioned samples obtained from the fibrosa layer of natural porcine AVs. An example of such images was presented in Figure 3. As discussed earlier, the AV tissue, and the distribution of the collagen fibrils within the tissue, are widely considered as planar. However, it may be the case that some fibrils may not be deposited in a single plane, and therefore the whole fibril length may not be captured in that optical plane. Should this be the case, the rationale of the presented analysis and the trend of the results remain unaffected, but rather the calculated numerical values may be scaled by the ratio of the whole fibril length to the length captured in the image. However, the values related to the fibril geometry presented in this study are well consistent with the reported values in the literature [26, 38, 39], reaffirming that the potential effects of non-planar fibrils on the presented calculations have been minimal.

### **Failure characteristics of the BHV versus the native AV**

Glutaraldehyde fixation notably alters the fibril interface shear and subsequently the critical length. Change in the critical length affects the population fraction of the fibrils that would be able to provide effective reinforcement and load-bearing to the tissue. By assuming a Gaussian distribution for the straight length  $l$  of the entire fibril population in the natural tissue:

$$D(l) = \frac{1}{\sigma_l \sqrt{2\pi}} \exp\left(-\frac{(l - \mu_l)^2}{2\sigma_l^2}\right) \quad (7)$$

where  $\mu_l$  and  $\sigma_l$  are the mean straight fibril length and the standard deviation, respectively; the fraction of the population of fibrils providing effective reinforcement to the tissue can be calculated by integrating the area underneath the distribution curve, from the critical length to the end tail of the distribution. Values for  $\mu_l$  and  $\sigma_l$  can be determined by first finding the straight fibril length of the residing population. If the wavy profile of a fibril is represented by

a mathematical function  $y$ , the straight length  $l$  of a fibril is established by

$l = \int_0^{l_0} \sqrt{1 + \left(\frac{dy}{dx}\right)^2} dx$ . Therefore, the straight length of the individual fibrils may be calculated

by fitting the extracted  $x$  and  $y$  coordinates of the way profiles of the individual fibrils obtained from our image processing analyses (e.g. Figure 3e) to mathematical functions that accurately represent the shape of the fibrils.

Using the coordinates of the initial and final points of the identified profile of a fibril, the angle  $\theta$  between the axis of that fibril and the horizontal axis was established. Using the rotation matrix  $R(\theta) = \begin{bmatrix} \cos \theta & -\sin \theta \\ \sin \theta & \cos \theta \end{bmatrix}$ , the extracted coordinates of the points along the wavy profile of each fibril were transformed to new coordinates, in-line with the global  $x$  and  $y$  axes. This transformation is shown schematically in Figure 4a. The transformed  $x$  and  $y$  coordinates were then fitted to a cubic spline function constructed of a piecewise third-order polynomial of the form:

$$y_i = a_i x^3 + b_i x^2 + c_i x + d_i, \quad 1 \leq i \leq n-1 \quad (8)$$

where  $a$ ,  $b$ ,  $c$  and  $d$  are fitting parameters,  $i$  indicates the subset of the function fitted to each piece of the experimental dataset (note that each piece contains four sets of points), and  $n$  is the total number of points that the function  $y_i$  is fitted to on its entire domain. The fitting procedure was performed using a customised code in MATLAB<sup>®</sup>, and a typical output is presented in Figure 4a. Upon calculation of  $a_i$ ,  $b_i$ ,  $c_i$  and  $d_i$ , the straight length  $l$  of each fibril was found by:

$$l = \sum_{i=1}^{n-1} \int_{x_i}^{x_{i+1}} \sqrt{1 + \left(\frac{dy_i}{dx}\right)^2} dx \quad (9)$$

From this data, the mean straight length and the standard deviation of the fibril population were obtained to be  $\mu_l = 68.80 \mu\text{m}$  and  $\sigma_l = 13.00 \mu\text{m}$ , respectively.

The distribution of the straight length  $l$  of the entire fibril population in the natural tissue may be retrieved by substituting the values of  $\mu_l$  and  $\sigma_l$  into  $D(l)$ , as

$D(l) = \frac{1}{13 \times \sqrt{2\pi}} \exp\left(-\frac{(l - 68.80)^2}{2 \times (13)^2}\right)$  and is shown in Figure 4b. The difference between the

fraction of the populations of fibrils effectively contributing to the load-bearing capacity of

BHV and natural AV tissues may now be obtained by  $\int_{25.36}^{66.81} D(l) dl$ , which results in:

$$\int_{25.36}^{66.81} \frac{1}{13 \times \sqrt{2\pi}} \exp\left(-\frac{(l - 68.80)^2}{2 \times (13)^2}\right) dl = 0.44.$$

Calculations therefore indicate a reduction of 44% in the population of fibrils that provide effective reinforcement to the BHV tissue compared with the natural valve. Such reduction is expected to inevitably affect and reduce the ultimate strength of the BHV. Interestingly, Lee et al. (1984) and Purinya et al. (1994) report experimental data which show ultimate failure stress of fixed tissues reduces by 40% to 50% compared with the samples from natural tissue [4, 5]. This observation is in close accordance with the above calculated 44% reduction in the population of load-bearing fibrils in the BHV tissue, underlining a direct correlation between the reduction in the ultimate failure strength and the fibril population that effectively contribute to the load-bearing capacity of the tissue. Therefore, the incurred changes on the magnitude of shear force acting on BHV fibril interfaces as a result of glutaraldehyde fixation (versus the natural tissue) alter the fibrils' critical length. Consequently, the fraction population of the load-bearing fibrils is reduced, which in turn decreases the ultimate failure strength of the BHV.

The fatigue-induced structural failure mode of the BHV tissue has shown to be of the form of delamination between collagen fibre layers, while the fibres themselves remain intact [10, 12]. This delamination implies that the shear forces acting on fibrils' interface were insufficient to exceed the fibrils' failure strength but sufficient to break the bonds between the fibril and the surrounding ECM proteins including the neighbouring fibrils. Therefore, quantitative estimations of the total bonding force acting on a fibril's lateral surface along its length, and the fibril failure load, are required. A collagen fibril is typically bonded to its surrounding ECM proteins via electrostatic bonds with GAG chains, and covalent bonds with the neighbouring fibrils, shown schematically in Figure 5. The fibril-GAG bonding occurs every 68 nm along the length of the fibril [39], with each bond proficient to sustain forces in order of ~50 pN [20]. The bonding of a collagen fibril with the surrounding fibrils is thought to occur in specific sites in each *D*-period along its length ( $D = 67$  nm), with each bond capable of withstanding ~6.1 nN before breaking [20]. The exact number of bonds and crosslinks between a fibril and its surrounding ECM proteins in native AV or fixed tissue along a fibril is unknown to the best knowledge of the authors. Aspden showed that

considering one bond per each bonding site suffices for the transmission of stress from the matrix to a fibril [20]. Balguid et al. (2007) have shown a linear correlation between the number of fibrillar crosslinks and the elastic modulus of a fibril [40]. As the estimated value for elastic modulus of cross-linked fibril is up to approximately 500 MPa versus 101.22 MPa for a residing fibril in the natural valve, the number of cross-links in a fixed tissue is assumed to increase proportionally by a factor of 5. Therefore, assuming 5 covalent bonds per each bonding site along a fibril and that the fibril-GAG bonds are not altered, the total force  $f$  acting on a fibril's interface (i.e. lateral surface) that is borne by the fibril-fibril and the fibril-GAG bonds is calculated by:

$$f = 5 \times \frac{\mu_l}{D} \times 6.1 \times 10^{-9} + \frac{\mu_l}{68 \times 10^{-9}} \times 50 \times 10^{-12} \quad (10)$$

Considering that the average length of fibril is 68.80  $\mu\text{m}$ ,  $f$  assumes a value of approximately  $f = 31 \mu\text{N}$ .

The shear force ( $F$ ) acting on the lateral surface of a cross-linked fibril before failure, noting that  $\sigma_{failure} = E\varepsilon_{failure}$  and  $\tau = \frac{F}{A_{lateral}}$ , is thus calculated using equation (5) as  $F = 38 \mu\text{N}$ . It is observed that the force  $f$  required to fail bonds between fibrils is critically lower than the force  $F$  required to break a fibril. Weaker bonds must therefore progressively break in BHV's functioning cycles, culminating in the so called fibril delamination from the matrix, while the fibril themselves remain intact.

## Conclusion and implication for BHV fabrication

Fibril critical length, bonding forces, and load-bearing populations in both natural AV and BHV tissues were calculated and presented in this paper for the first time, to the knowledge of the authors. While some studies suggest that the fibrils residing in the different morphological layers of the native AV and the BHV may sustain various levels of shear under tissue-level deformations [41], the calculated values reported in the paper can be considered as typical whole-tissue values.

It was shown that the microstructural changes incurred in the valve ECM as a result of glutaraldehyde fixation inevitably result in changes to the fibril interface shear and critical length. By calculating these changes, this paper provided a prediction of the tissue failure

properties which corroborates the experimental observations. The presented analysis in this paper provides a quantitative insight into the biomechanics of the changes that occur in the fibril-level due to tissue fixation, and facilitates further understanding of the ensuing microstructural causes that initiate the degeneration of the BHVs *in vivo*.

The results of these analyses suggest that BHV fabrication methods which include tissue fixation are potentially undesirable if the aim is to prolong the durability of the replaced valve function *in vivo*. Indeed, any chemical treatment of BHV tissue is highly likely to alter the nature of the fibril-matrix interactions, the ensuing shear stress and therefore the biomechanical properties of the valve as presented here. An alternative approach, as an initial concept, may be the utilisation of a flexible biocompatible nano-sheath film to cover the surface of a natural AV leaflet, in order to prevent any immunological and biological reactions, while maintaining the natural structure and properties of the native valve. The outcomes of this study may be used to recommend appropriate choice of objective functions in optimising the design of such sheath, and the modelling of the sheathed valve function. For example, designs to minimise the fibril interface shear in sheathed versus normal valve can be proposed. This approach therefore facilitates designing more desirable valve substitutes with prolonged functional durability.

## Appendix A

Plotting  $\log \dot{\lambda}$  versus  $\log \eta$  in Figure A1 for the three experimentally quantified  $(\dot{\lambda}, \eta)$  data points, it may be observed that each two consecutive points have notably different gradients. This implies that at least two exponential terms may be required to adequately describe the behaviour of  $\eta$  versus  $\dot{\lambda}$  via an exponential profile, over the whole range of the three existing points. This function may be mathematically expressed as:

$$\eta(\dot{\lambda}) = a \exp b \dot{\lambda} + c \exp d \dot{\lambda} \quad (\text{A1})$$

where  $a$ ,  $b$ ,  $c$  and  $d$  are constants to be calculated by fitting this function to the data points.

Setting the first exponential term in equation (A1) to describe the  $\eta$ - $\dot{\lambda}$  behaviour of the first two points, and accepting fits with  $R^2 \geq 0.99$  using MATLAB<sup>®</sup>, domains for  $a$  and  $b$  over which acceptable fits may be achieved were obtained to be  $740 \leq a \leq 850$  and  $-200 \leq b \leq -140$ , respectively. These provided the numerical constraints for fitting equation (A1) to all three  $(\dot{\lambda}, \eta)$  points:

$$\eta(\dot{\lambda}) = a \exp b \dot{\lambda} + c \exp d \dot{\lambda}, \quad \begin{cases} 740 \leq a \leq 850 \\ -200 \leq b \leq -140 \end{cases} \quad (\text{A2})$$

However, another constraint is derived from the rheological properties of GAG. The yield stress of GAG solutions has been reported to be lower than  $10^5$  Pa [42]. Assuming that  $\tau$  is in the range of  $10^4 \text{ Pa} \leq \tau \leq 10^5 \text{ Pa}$ , the model parameters in (A2) should provide the best fit to the three  $(\dot{\lambda}, \eta)$  points such that the corresponding value of  $\eta$  at  $\dot{\lambda} = 2.5 \text{ s}^{-1}$  establishes that  $10^4 \leq 2\eta \frac{\dot{\lambda}}{\lambda}$ . Therefore equation (A2) is rewritten as:

$$\eta(\dot{\lambda}) = a \exp b \dot{\lambda} + c \exp d \dot{\lambda}, \quad \begin{cases} 740 \leq a \leq 850 \\ -200 \leq b \leq -140 \\ 10^4 \leq 2\eta \frac{\dot{\lambda}}{\lambda} \end{cases} \quad (\text{A3})$$

Fitting equation (A3) to the data points, the set of  $a$ ,  $b$ ,  $c$  and  $d$  that provided  $R^2 = 1$  while satisfying those constraints were calculated to be:  $a = 778.7$ ,  $b = -180.3$ ,  $c = 24.89$ , and  $d = -2.97$ :

$$\eta(\dot{\lambda}) = 778.7 \exp(-180.3\dot{\lambda}) + 24.89 \exp(-2.97\dot{\lambda}) \quad (\text{A4})$$

where the lower bound for  $\eta$  at  $\dot{\lambda} = 2.5$  was estimated to be  $\eta = 0.0145$  MPa s.

## References

1. Broom ND. The stress/strain and fatigue behaviour of glutaraldehyde preserved heart-valve tissue. *J Biomech.* 1977; 10(11): 707-24.
2. Thubrikar M, Piepgrass WC, Deck JD, Nolan SP. Stresses of natural versus prosthetic aortic valve leaflets in vivo. *Ann Thorac Surg.* 1980; 30(3): 230-9.
3. Billiar KL, Sacks MS. Biaxial mechanical properties of the natural and glutaraldehyde treated aortic valve cusp - Part I: Experimental results. *J Biomech Eng.* 2000; 122(1): 23-30.
4. Lee JM, Boughner DR, Courtman DW. The glutaraldehyde-stabilized porcine aortic valve xenograft. II. Effect of fixation with or without pressure on the tensile viscoelastic properties of the leaflet material. *J Biomed Mater Res.* 1984; 18(1): 79-98.
5. Purinya B, Kasyanov V, Volkolakov J, Latsis R, Tetere G. Biomechanical and structural properties of the explanted bioprosthetic valve leaflets. *J Biomech.* 1994; 27(1): 1-11.
6. Vesely I, Barber JE, Ratliff NB. Tissue damage and calcification may be independent mechanisms of bioprosthetic heart valve failure. *J Heart Valve Dis.* 2001; 10(4): 471-77.
7. Sacks MS. The biomechanical effects of fatigue on the porcine bioprosthetic heart valve. 2001. *J Long Term Eff Med Implants.* 2001; 11(3-4): 231-47.
8. Schoen FJ, Levy RJ. Calcification of tissue heart valve substitutes: progress toward understanding and prevention. *Ann Thorac Surg.* 2005; 79(3): 1072-80.
9. Pibarot P, Dumesnil JG. Valvular heart disease: Changing concepts in disease management. *Circulation.* 2009; 119, 1034-1048.
10. Sacks MS, Schoen FJ. Collagen fiber disruption occurs independent of calcification in clinically explanted bioprosthetic heart valves. *J Biomed Mater Res.* 2002; 62(3): 359-71.
11. Wells SM, Sacks MS. Effects of pressure on the biaxial mechanical behaviour of porcine bioprosthetic heart valves with long-term cyclic loading. *Biomaterials.* 2002; 23(11): 2389-2399.
12. Mirnajafi A, Zubiato B, Sacks MS. Effects of cyclic flexural fatigue on porcine bioprosthetic heart valve heterograft biomaterials. *J Biomed Mater Res A.* 2010; 94(1): 205-13.
13. Sacks MS, Merryman WD, Schmidt DE. On the biomechanics of heart valve function. *J Biomech.* 2009; 42(12): 1804-1824.
14. Lewinsohn AD, Anssari-Benham A, Lee DA, Taylor PM, Chester AH, Yacoub MH, Screen HRC. Anisotropic strain transfer through the aortic valve and its relevance to the cellular mechanical environment. *Proc Inst Mech Eng H.* 2011; 225(8): 821-30.
15. Vesely I. Heart valve tissue engineering. *Circulation Research.* 2005; 97(8): 743-755.
16. Stella JA, Sacks MS. On the biaxial mechanical properties of the layers of the aortic valve leaflet. *J Biomech Eng.* 2007; 129(5): 757-766.
17. Anssari-Benam A, Bader DL, Screen HRC. A combined experimental and modelling approach to aortic valve viscoelasticity in tensile deformation. *J Mater Sci Mater Med.* 2011; 22(2): 253-62.

18. Billiar KL, Sacks MS. Biaxial mechanical properties of the natural and glutaraldehyde treated aortic valve cusp – part II: a structural constitutive model. *J Biomech Eng.* 2000; 122(4): 327-35.
19. Sacks MS. Incorporation of experimentally derived fiber orientation into a structural constitutive model for planar collagenous tissues. *J Biomech Eng.* 2003; 125(2): 280-7.
20. Aspden RM. Fibre reinforcing by collagen in cartilage and soft connective tissues. *Proc Biol Sci.* 1994; 258(1352): 195-200.
21. Aspden RM. Fibre stress and strain in fibre-reinforced composites. *J Mat Sci.* 1994; 29(5): 1310-1318.
22. Goh KL, Aspden RM, Hukins DWL. Critical length of collagen fibrils in extracellular matrix. *J Theor Biol.* 2003; 223(2): 259-61.
23. Kato YP, Christiansen DL, Hahn RA, Shieh S-J, Goldstein JD, Silver FH. Mechanical properties of collagen fibres: a comparison of reconstituted and rat tail tendon fibres. *Biomaterials.* 1989; 10(1): 38-42.
24. Sasaki N, Odajima S. Elongation mechanism of collagen fibrils and force-strain relations of tendon at each level of structural hierarchy. *J Biomech.* 1996; 29(9): 1131-6.
25. Gentleman E, Lay AN, Dickerson DA, Nauman EA, Livesay GA, Dee KC. Mechanical characterization of collagen fibers and scaffolds for tissue engineering. *Biomaterials.* 2003; 24(21): 3805-13.
26. Gautieri A, Vesentini S, Redaelli A, Buehler MJ. Hierarchical structure and nanomechanics of collagen microfibrils from the atomistic scale up. *Nano Letters.* 2011; 11(2): 757-66.
27. Hang F, Barber AH. Nano-mechanical properties of individual mineralized collagen fibrils from bone tissue. *J R Soc Interface.* 2011; 8(57): 500-5.
28. Ahmadzadeh H, Connizzo BK, Freedman BR, Soslowky LJ, Shenoy VB. Determining the contribution of glycosaminoglycans to tendon mechanical properties with a modified shear-lag model. *J Biomech.* 2013; 46(14): 2497 - 2503.
29. Filon LNG. On the elastic equilibrium of circular cylinders under certain practical systems of load. *Phil Trans Royal Soc Lond A.* 1902; 198(300): 147-233.
30. Gupta HS, Seto J, Krauss S, Boesecke P, Screen HRC. In situ multi-level analysis of viscoelastic deformation mechanisms in tendon collagen. *J Struct Biol.* 2010; 169(2): 183-91.
- 31- Anssari-Benam A, Bader DL, Screen HRC. Anisotropic time-dependant behaviour of the aortic valve. *J Mech Behav Biomed Mater.* 2011; 4(8): 1603-10.
- 32- Leeson-Dietrich J, Boughner D, Vesely I. Porcine pulmonary and aortic valves: a comparison of their tensile viscoelastic properties at physiological strain rates. *J Heart Valve Dis.* 1995; 4(1): 88-94.
33. Thubrikar M, Aouad J, Nolan SP. Comparison of the in-vivo and in-vitro mechanical properties of aortic valve leaflets. *J Thorac Cardiovasc Surg.* 1986; 92(1): 29-36.

34. Liao J, Yang L, Grashow J, Sacks MS. The relation between collagen fibril kinematics and mechanical properties in the mitral valve anterior leaflet. *J Biomech Eng.* 2007; 129(1): 78-87.
35. Parry DAD, Barnes GRG, Craig AS. A comparison of the size distribution of collagen fibrils in connective tissues as a function of age and a possible relation between fibril size distribution and mechanical properties. *Proc R Soc Lond B Biol Sci.* 1978; 203(1152): 305-21.
36. Taylor PM. Biological matrices and bionanotechnology. *Philos Trans R Soc Lond B Biol Sci.* 2007; 362(1484): 1313-20.
37. Pins GD, Christiansen DL, Patel R, Silver FH. Self-assembly of collagen fibers. Influence of fibrillar alignment and Decorin on mechanical properties. *Biophys J.* 1997; 73(4): 2164-72.
38. Craig AS, Birtles MJ, Conway JF, Parry DA. An estimate of the mean length of collagen fibrils in rat tail-tendon as a function of age. *Connect Tissue Res.* 1989; 19(1): 51-62.
39. Redaelli A, Vesentini S, Soncini M, Vena P, Mantero S, Montecvecchi FM. Possible role of decorin glycosaminoglycans in fibril to fibril force transfer in relative mature tendons - a computational study from molecular to microstructural level. *J Biomech.* 2003; 36(10): 1555-69.
40. Balguid A, Rubbens MP, Mol A, Bank RA, Bogers AJ, van Kats JP, de Mol BA, Baaijens FP, Bouten CV. The role of collagen cross-links in biomechanical behavior of human aortic heart valve leaflets - relevance for tissue engineering. *Tissue Eng.* 2007; 13(7): 1501-11.
- 41- Anssari-Benam A, Gupta HS, Screen HRC. Strain transfer through the aortic valve. *J Biomech Eng.* 2012; 134(6), 061003, doi: 10.1115/1.4006812.
- 42- Hukins DWL, Aspden RM, Yarker YE. Fibre reinforcement and mechanical stability in articular cartilage. *Eng Med.* 1984; 13(3): 153-6.

## Figure legends

**Figure 1-** Schematic of AV anatomy and structure: (a) schematic cross-section of heart; (b) AV located at the aortic root (adapted from [13] with permission); (c) AV cut open showing the valve's three leaflets (adapted from [14] with permission); (d) an intact AV leaflet with its principal loading directions; and (e) schematic of the AV structure as a fibre-reinforced composite material: collagen fibrils are embedded in GAG as ground substance (adapted from [15], with permission).

**Figure 2-** (a) Variation in  $\eta$  versus  $\dot{\lambda}$ . The value of  $\eta$  at physiological rate ( $\dot{\lambda} = 2.5 \text{ s}^{-1}$ ) was estimated by fitting the existing  $(\dot{\lambda}, \eta)$  points to the bi-exponential function expressed in (A4). The  $(\dot{\lambda}, \eta)$  points were collated from [17]; (b) Representative example of variation in  $\eta$  for natural versus fixed tissue (experimental data collated from [2]). Note the approximately 5-fold increase in the value of  $\eta$  for the fixed tissue compared with the natural valve.

**Figure 3-** (a) A typical pre-processed histological image of natural AV specimens obtained using conventional light microscopy; (b) A typical post-processed image. A region of interest is designated by the dashed rectangle. For each region of interest, histograms of fibril radius (c) and crimped length (d) of the residing population of fibrils were obtained, along with the  $x$  and  $y$  coordinates of the profile of the wavy fibrils (e). The scale bar on the histological image indicates  $100 \mu\text{m}$ .

**Figure 4-** (a) The angle  $\theta$  between the axis of a fibril and the horizontal axis was calculated for each fibril, and used in the rotation matrix  $R(\theta)$  to transform the extracted coordinates of the points from the initial profile of the fibrils new coordinates in-line with the global  $x$  and  $y$  axes. The new points (shown by filled circles in the bottom panel) were then fitted to the function in equation (8), shown by continuous line. Using equation (9), the straight length of the fibrils was then calculated. For the specific fibril shown in the figure,  $l = 79.92 \mu\text{m}$  (indicated by dashed line); (b) The Gaussian distribution of the straight length of the fibril population in natural AV tissue. Dashed lines indicate the critical lengths of the natural versus fixed BHV tissue. The hatched area corresponds to the difference between the fraction of the populations of fibrils providing effective reinforcement and load-bearing to BHV and natural AV tissues.

**Figure 5-** Schematic of the bonding between a fibril and the surrounding ECM proteins in AV, including GAG and a neighbouring fibril.

**Figure A1-**  $\eta$  versus  $\dot{\lambda}$  plotted in logarithmic scale. The connecting dashed lines between each two consecutive points highlight the respective gradients. Note the ~30% difference in the gradient values.

**Figure 1**

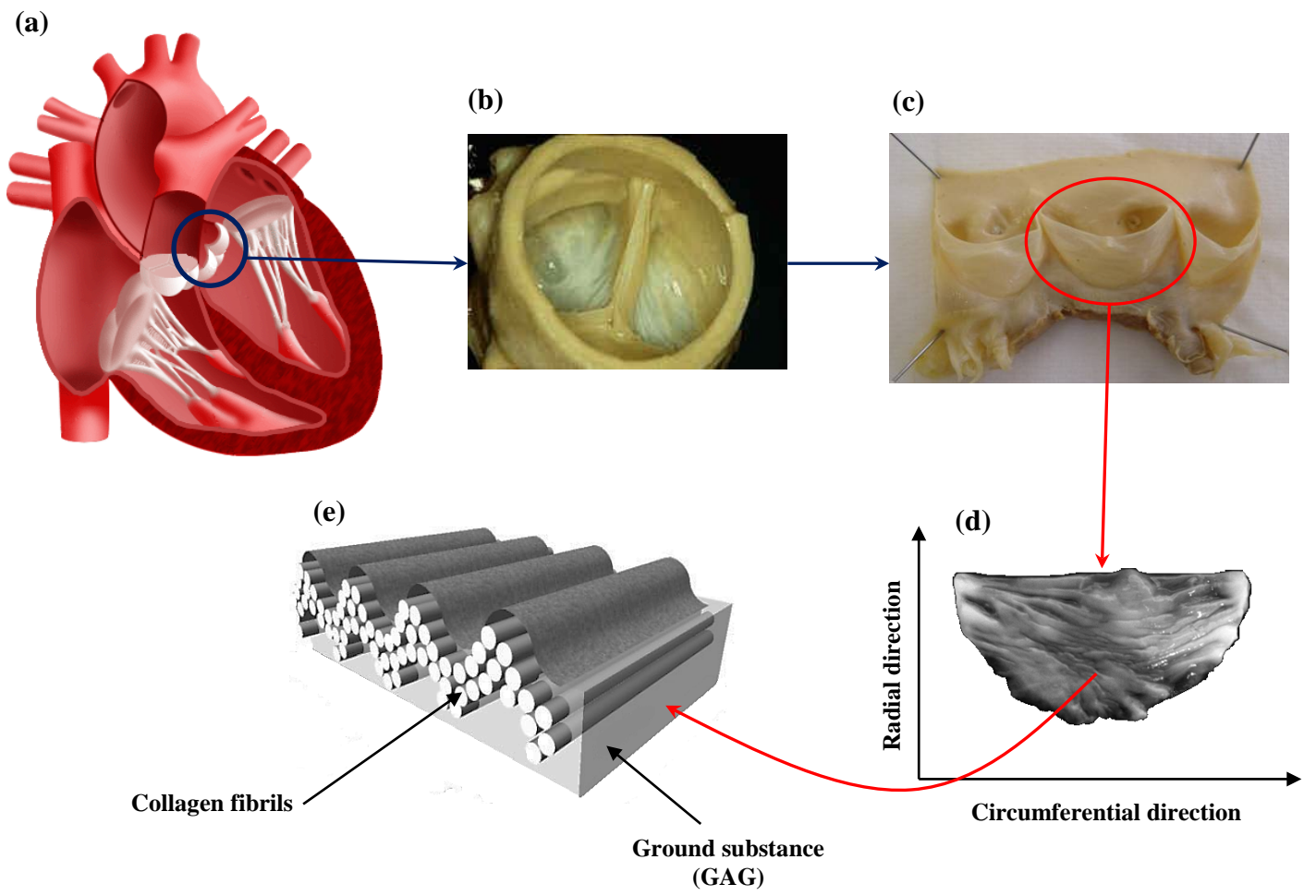
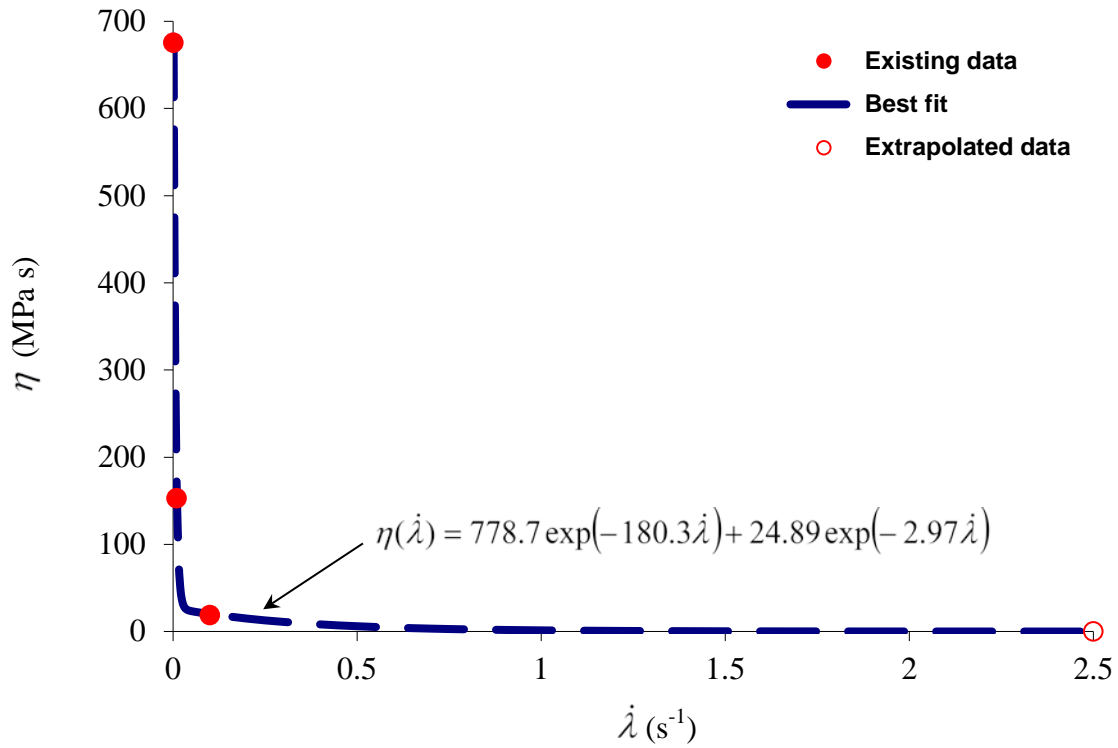


**Figure 2**

**(a)**



**(b)**

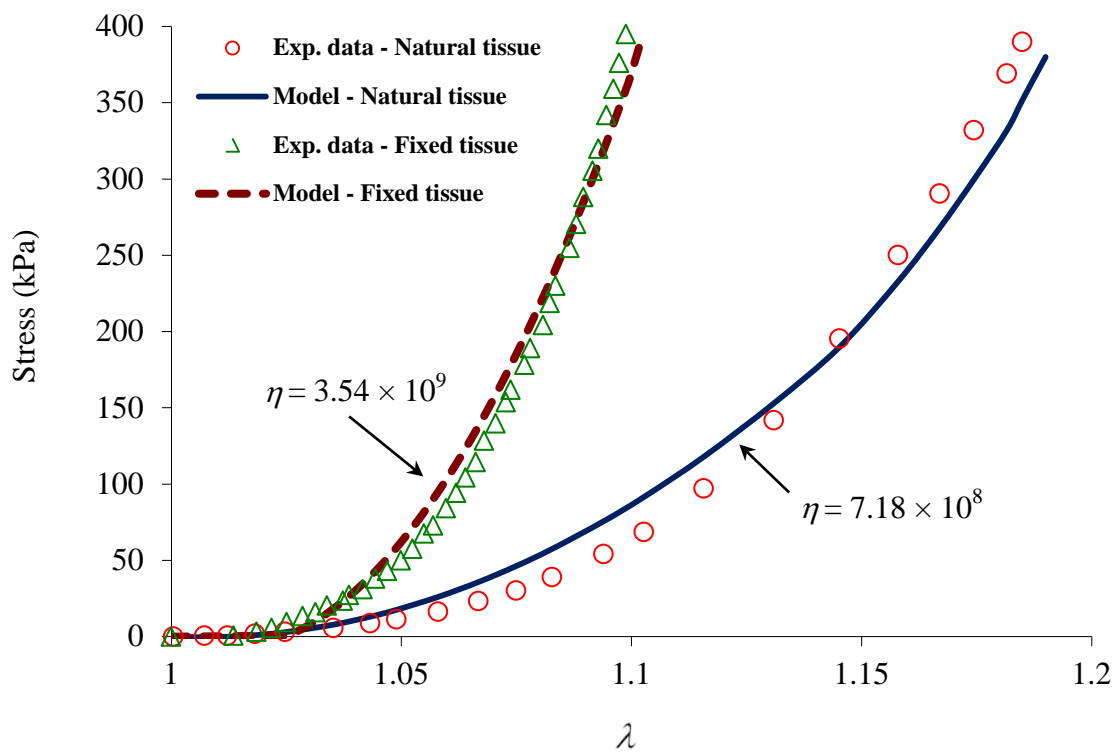


**Figure 3**

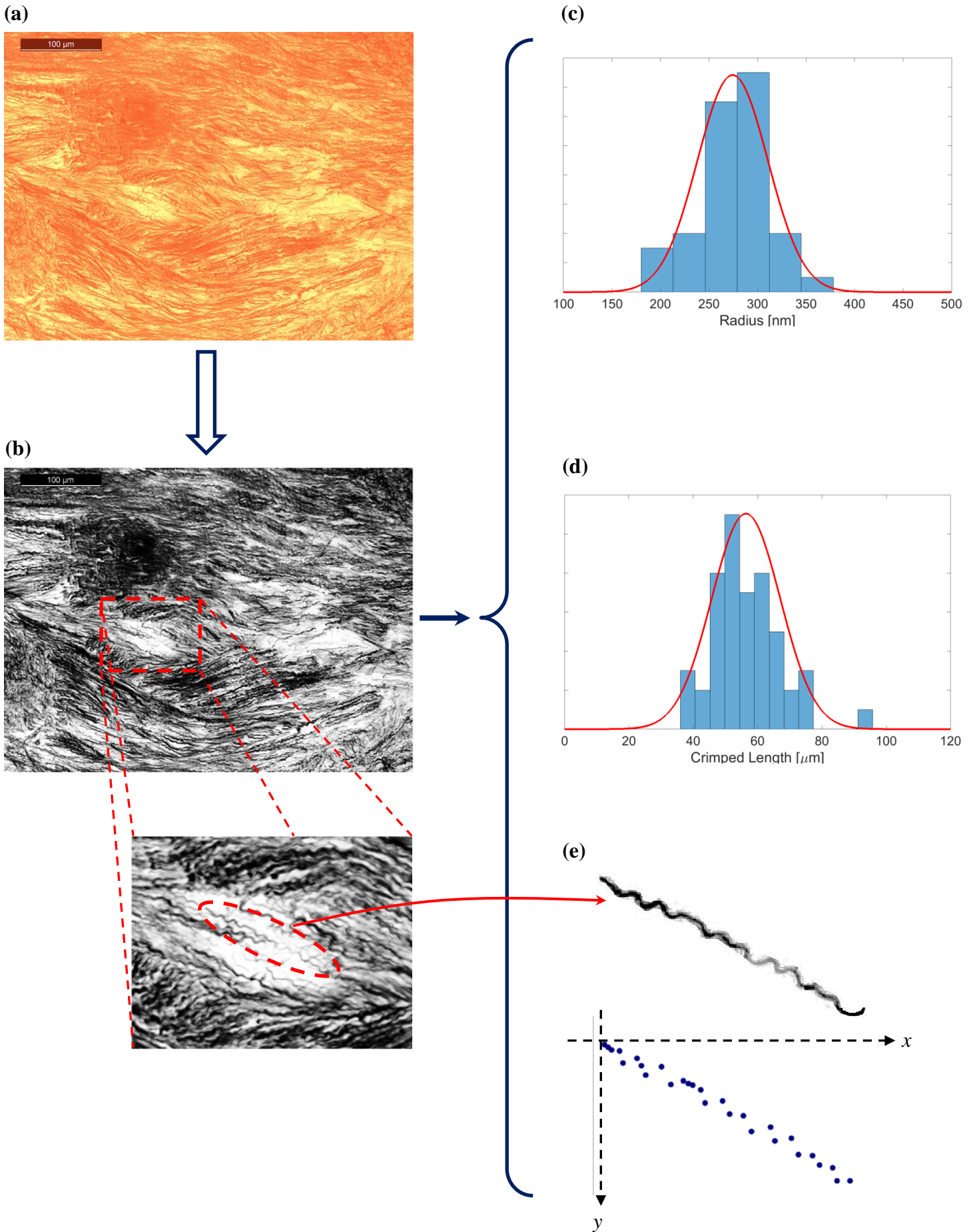
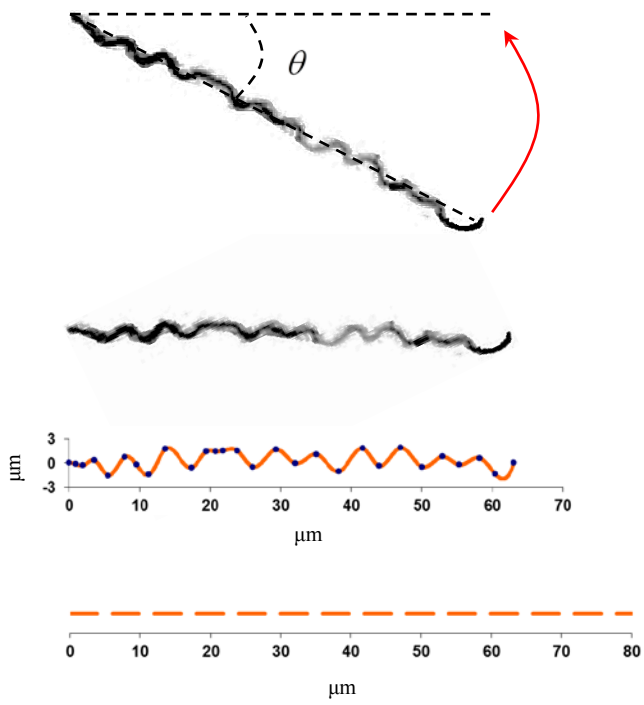


**Figure 4**

**(a)**



**(b)**

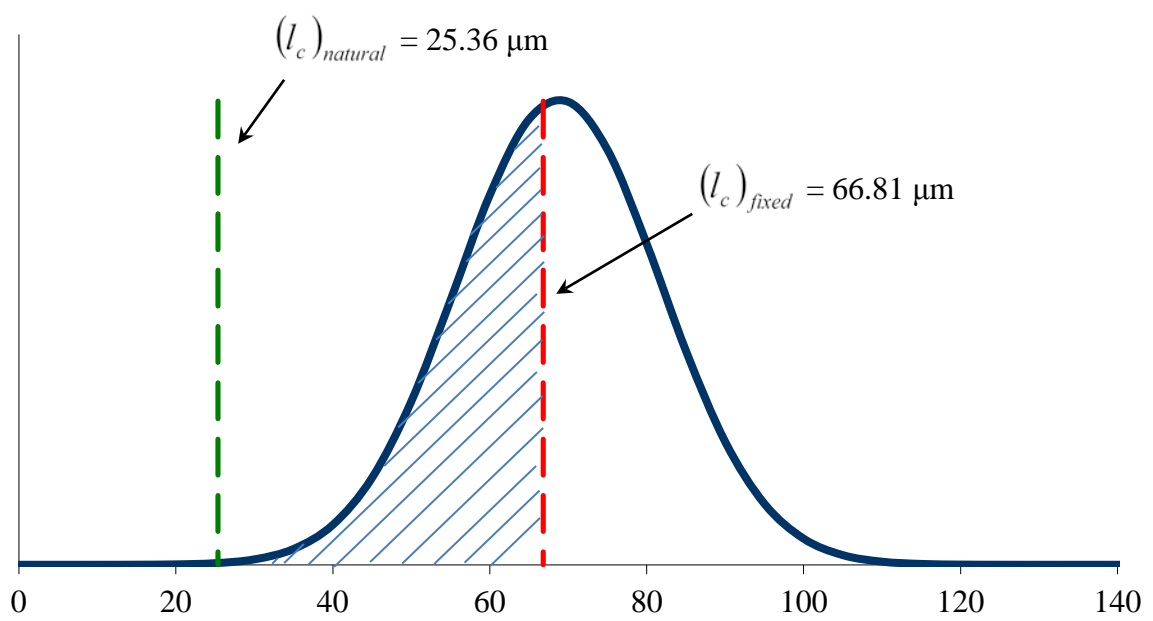


**Figure 5**

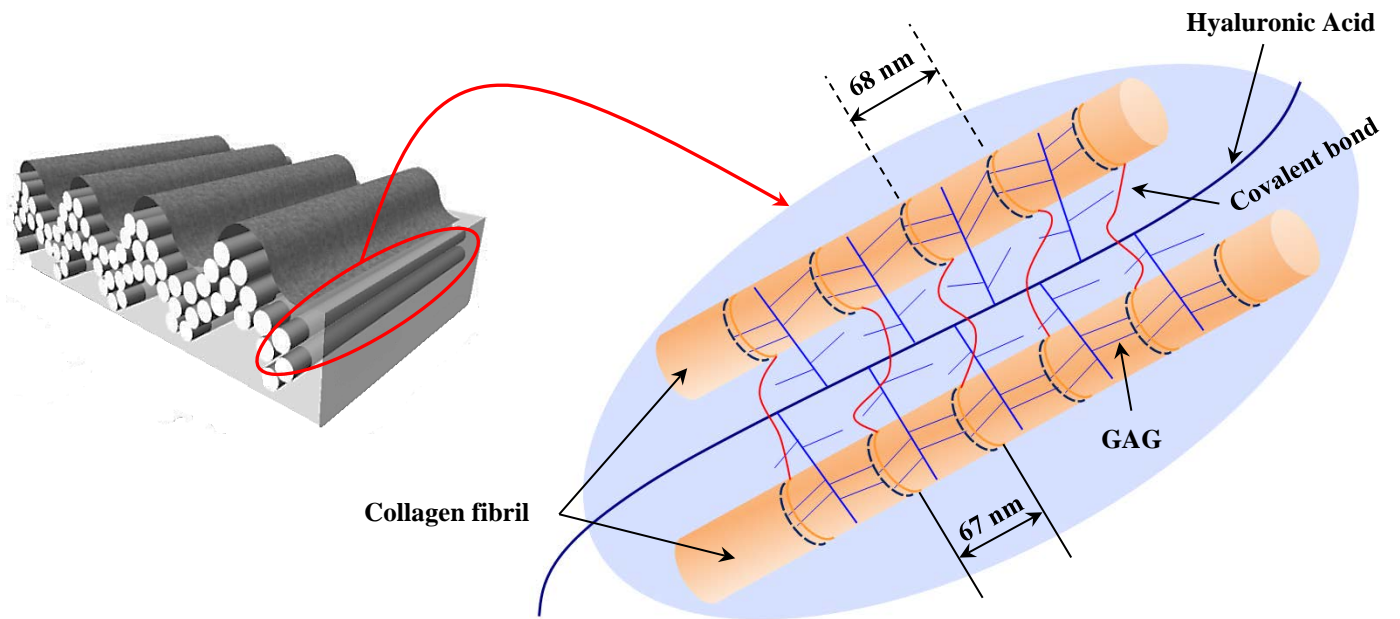


**Figure A1**

